Postprint of: Mielewczyk-Gryń A., Yang S., Balaguer M., Strandbakke R., Sørby M. H., Szpunar I., Witkowska A., Wachowski S., Serra J. M., Navrotsky A., Gazda M., Energetics of formation and stability in high pressure steam of barium lanthanide cobaltite double perovskites, DALTON TRANSACTIONS, Vol. 52, iss. 17 (2023), pp. 5771-5779, DOI: 10.1039/D2DT03989C

Energetics of formation and stability in high pressure steam of barium lanthanide cobaltite double perovskites

Received 00th January 20xx,
Accepted 00th January 20xx

DOI: 10.1039/x0xx00000x

Aleksandra Mielewczyk-Gryń[a*], Shuhao Yang[b, †], Maria Balaguer[c], Ragnar Strandbakke[d], Magnus H. Sørby[e], Iga Szpunar[a], Agnieszka Witkowska[a], Sebastian Wachowski[a], Jose M. Serra[c], Alexandra Navrotsky[b], and Maria Gazda[a]

This study concerns energetics of formation and the stability in high water partial pressure of $BaLnCo_2O_{6-\delta}$, (Ln = La, Pr, Nd, and Gd) (BLnC) and $BaGd_{1-x}La_xCo_2O_{6-\delta}$, where x = 0.2, 0.5, and 0.7 (BGLC) double perovskite cobaltites. Those materials are extensively studied due to their potential applications as a positrode in electrochemical devices. Therefore, their stability under such conditions is a key issue. All investigated materials are thermodynamically stable relative to binary oxides and exhibit strongly exothermic enthalpies of formation. Moreover, $BaGd_{0.3}La_{0.7}Co_2O_{6-\delta}$ and $BaGd_{0.8}La_{0.2}Co_2O_{6-\delta}$ remain the main perovskite structure up to 3 bars of water vapor at 400 °C. At higher steam pressure, reaching 10 bar at 300 °C, the partial decomposition to constituent oxides and hydroxides was observed. The BGLC compounds exhibit higher negative formation enthalpies in comparison to single-Ln compositions, which does not translate into higher chemical stability under high steam pressures since the BLnC series retained the main perovskite structure at higher temperatures as well as in higher water vapor pressures.

Introduction

Ba- and Co-based double perovskites have a variety of applications in electrical and electrochemical devices and are increasingly investigated as positrodes (positive electrodes) in protonic ceramic electrochemical cells (PCECs), comprising proton ceramic fuel cells (PCFCs) and electrolyzers (PCEs).[1–3] In PCEs, the chemical stability of materials under high steam pressures is of the essence, but there are few relevant studies[4,5]. Recently, multiple properties of double perovskites with the formula BLnCs, referring to a perovskite with a mix of divalent Ba and one or two trivalent lanthanides (Ln) occupying A-sites have been evaluated, including structure, hydration behavior, and electrochemical performance.[6–10] In the present work, the thermodynamic stability of these materials has been studied by high-temperature oxide melt solution calorimetry, and the stability at high steam pressures was validated by X-ray diffraction after long-term exposure. These studies aimed to provide new insights into the fundamentals of the energetic stability of barium lanthanide cobaltites to guide their applicability as positrodes in PCECs.

Experimental

Commercial $BaGd_{0.3}La_{0.7}Co_2O_{6-\delta}$ (BGLC37) and $BaGd_{0.8}La_{0.2}Co_2O_{6-\delta}$ (BGLC82) (Marion Technologies) (BGLCs) were used in this study. Additional samples with one lanthanide (BLnC), namely $BaNdCo_2O_{6-\delta}$ (BNC), $BaPrCo_2O_{6-\delta}$ (BPC), and $BaLaCo_2O_{6-\delta}$ (BLC), $BaGdCo_2O_{6-\delta}$ (BGC), as well as $BaGd_{0.5}La_{0.5}Co_2O_{6-\delta}$ (BGLC55), were synthesized by solid state reactions and described in our previous works.[6,7] The oxidation state of cobalt was determined using iodometric titration at room temperature, in which approximately 15–20 mg of each sample was used. Details of the experimental procedure can be found elsewhere.[11] Powder X-ray diffraction (PXRD) patterns were obtained using a Bruker D2 Phaser diffractometer operated with Cu Kα radiation (λ = 1.54184 Å), 3.0 mm air scatter screen, and 1.0 mm divergence slit. The data were collected in the 2θ range of 10–80° with a step size of 0.02° and a dwell time of 0.8 s per step. Lattice parameters were refined based on peak positions in the PXRD patterns using MDI Jade software. High temperature oxide melt solution calorimetry experiments were carried out using a Setaram AlexSYS Tian-Calvet twin microcalorimeter following the standard method described previously.[12] The calorimeter was calibrated against the heat content of high-purity α-Al_2O_3 (99.99%). Pressed sample pellets (~5 mg) were dropped from ambient temperature into the calorimeter containing the solvent, molten sodium molybdate ($3Na_2O{\cdot}4MoO_3$), in a Pt crucible at 800 °C. The temperature has been chosen to ensure complete

[a.] *Institute of Nanotechnology and Materials Engineering, Faculty of Applied Physics and Mathematics, and Advanced Materials Centre, Gdańsk University of Technology, Narutowicza 11/12 80-233 Gdańsk, Poland.*
[b.] *School of Molecular Sciences and Center for Materials of the Universe, Arizona State University, Tempe, AZ 85287, USA.*
[c.] *Instituto de Tecnología Química, Universitat Politècnica de València, Consejo Superior de Investigaciones Científicas, Av. Naranjos s/n, E-46022 Valencia, Spain.*
[d.] *Department of Chemistry, Centre for Materials Science and Nanotechnology (SMN), University of Oslo, Oslo, Norway*
[e.] *Institute for Energy Technology, Department for Hydrogen Technology, P.O. Box 40, Kjeller, 2027, Norway*
† Current address: *Energy Storage and Distributed Resources Division, Lawrence Berkeley National Laboratory, Berkeley, California 94720, United States*
Electronic Supplementary Information (ESI) available: [details of any supplementary information available should be included here]. See DOI: 10.1039/x0xx00000x

and fast dissolution of the material. All experiments were flushed with Ar at 60 mL min^{-1} with bubbling through the solvent at 5 mL min^{-1} to aid dissolution and prevent local saturation of the solvent. The thermodynamic cycles used to calculate enthalpies of formation from oxides ($\Delta H°_{f.\ ox}$) or elements ($\Delta H°_{f.\ el}$) are presented in Table 1, and the enthalpies of drop solution (ΔH_{ds}) for binary oxides are listed in Table 2.

Table 1. Thermodynamic cycles used to calculate the enthalpies of formation from oxides ($\Delta H°_{f.\ ox}$) or elements ($\Delta H°_{f.\ el}$) at 25 °C. s, soln, and g refer to solid, dissolved (in calorimetric solvent), and gaseous phases, respectively. *Drop solution (ΔH_{ds}) enthalpy values presented in Table 2

Reaction	ΔH (kJ mol^{-1})
$BaLnCo_2O_{6-\delta}$ (s, 25 °C) → BaO (soln, 800 °C) + $1/2Ln_2O_3$ (soln, 800 °C) + 2CoO (soln, 800 °C) + $(3/4-\delta/2)O_2$ (g, 800 °C)	$\Delta H_1 = \Delta H_{ds}$
BaO (s, 25 °C) → BaO (soln, 800 °C)	ΔH_2
Ln_2O_3 (s, 25 °C) → Ln_2O_3 (soln, 800 °C)	ΔH_3*
CoO (s, 25 °C) → CoO (soln, 800 °C)	ΔH_4
O_2 (g, 25 °C) → O_2 (g, 800 °C)	$\Delta H_5 = 25.27$ [13]
BaO (s, 25 °C) + $1/2Ln_2O_3$ (s, 25 °C) + 2CoO (s, 25 °C) + $(3/4-\delta/2)O_2$ (g, 25 °C) → $BaLnCo_2O_{6-\delta}$ (s, 25 °C)	$\Delta H°_{f,\ ox}$
$\Delta H°_{f,\ ox} = -\Delta H_1 + \Delta H_2 + 1/2\Delta H_3 + 2\Delta H_4 + (3/4-\delta/2)\Delta H_5$	
Ba (s, 25 °C) + $1/2O_2$ (g, 25 °C) → BaO (s, 25 °C)	ΔH_6
2Ln (s, 25 °C) + $3/2O_2$ (g, 25 °C) → Ln_2O_3 (s, 25 °C)	ΔH_7
Co (s, 25 °C) + $1/2O_2$ (g, 25 °C) → CoO (s, 25 °C)	ΔH_8
Ba (s, 25 °C) + Ln (s, 25 °C) + 2Co (s, 25 °C) + $(3-\delta/2)O_2$ (g, 25 °C) → $BaLnCo_2O_{6-\delta}$ (s, 25 °C)	$\Delta H°_{f,\ el}$
$\Delta H°_{f,\ el} = \Delta H°_{f,\ ox} + \Delta H_6 + 1/2\Delta H_7 + 2\Delta H_8$	

Table 2 Enthalpies of drop solution (ΔH_{ds}) in $3Na_2O{\cdot}4MoO_3$ at 800 °C and enthalpies of formation from elements ($\Delta H°_{f,\ el}$) at 25 °C for binary oxides.

Binary oxide	ΔH_{ds} (kJ mol^{-1})	$\Delta H°_{f,\ el}$ (kJ mol^{-1})
BaO	−176.48 ± 3.48 [14]	−548.1 ± 2.1 [13]
La_2O_3	−221.81 ± 2.25 [15]	−1791.6 ± 2.0 [16]
Pr_2O_3	−177.85 ± 8.21 [a]	−1809.9 ± 3.0 [16]
Nd_2O_3	−156.95 ± 1.05 [17]	−1806.9 ± 3.0 [16]
Gd_2O_3	−134.48 ± 1.70 [17]	−1830.9 ± 5.0 [18]
CoO	21.92 ± 0.36 [17]	−237.7 ± 0.4 [13]

[a] Based on the thermodynamic cycle listed in Table S1.

Stability tests under conditions of high water partial pressure and elevated temperature were performed in steel cells. The chemical stability of as-synthesized BLnC and BGLC (BGLC37 and BGLC82) powders was examined at two steam pressure conditions. The first involved 3 bars of total pressure, consisting of 1.5 bar of steam, 0.24 bar of oxygen, and 1.26 bar of Ar, at 400 °C for 72 h. In the high-pressure treatment, the total pressure was increased to 21 bar: 10.5 bar of steam, 1.68 bar of oxygen, and balanced with 8.82 bar of nitrogen, maintaining the temperature at 300 °C for 100 h. A third steam treatment was performed by rising the temperature to 600°C and maintaining atmospheric total pressure, consisting of 0.5 atm of steam, 0.08 atm of O_2, and 0.42 atm of Ar. The crystalline phases were analyzed by PXRD before and after the exposure. PXRD patterns were collected by a PANalytical Cubix fast diffractometer, using Cu Kα radiation (λ = 1.5406 Å) and an X'Celerator detector in Bragg–Brentano geometry. X-ray diffractograms were recorded in the 2θ range from 10° to 90° with a step size of 0.02°, which were analyzed using X'Pert Highscore Plus software.

Synchrotron radiation powder X-ray diffraction (SR-PXRD) was performed at the I11 beamline at the Diamond Light Source synchrotron (Didcot, UK). The instrument was equipped with 45 photomultiplier detectors each with a Si(111) analyzer crystal [19] and the wavelength was 0.82453 Å. The samples were placed in 0.3 mm borate glass capillaries which were spinning during data acquisition.

X-ray absorption spectroscopy (XAS) measurements were performed at the Solaris National Synchrotron Radiation Centre (Kraków, Poland). A dedicated photoemission electron microscope (PEEM)/XAS bending magnet beamline was utilized to measure oxygen K-edge spectra. Sample powders were mounted on carbon tape and placed on Omicron plates for measurements.

Results and discussion

Structural Information

Since the structure of barium lanthanide cobaltites has been discussed elsewhere,[6,7] this work focuses on chemical and structural differences, including chemical composition, lattice parameters, Co oxidization and spin states, and the phases

before and after high steam pressure stability tests. Figure 1 presents the PXRD patterns of as-prepared samples, confirming single phases for all compositions.

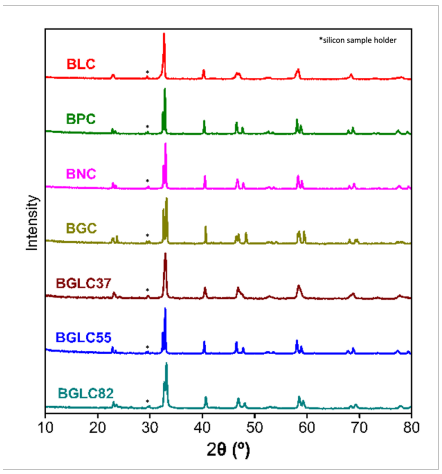

Figure 1. X-ray diffractograms of BLnCs and BGLCs as-prepared samples. Marked peak stems from the silicon XRD sample holder.

Besides the lattice shrinkage due to the decreasing Ln size as the atomic number increases, lattice parameters of BLnC's are also affected by oxygen stoichiometry associated with the Co oxidation state. To have a comprehensive consideration of ionic interactions, the structure factor of the Glasser–Jenkins equation[20] (SF_{GJ}) was used to differentiate studied samples. SF_{GJ} is defined as

$$\mathbf{SF_{GJ}} = \mathbf{I}\left(\frac{2\mathbf{I}}{\mathbf{V_m}}\right)^{\mathbf{1/3}} \qquad (1)$$

, where I is the ionic strength term, V_m is the molar unit cell volume – unit cell volume/formula units per unit cell, and $(2I/V_m)^{1/3}$ represents the cation-anion distance term. The ionic strength, I, can be calculated by

$$\mathbf{I} = \frac{\mathbf{1}}{\mathbf{2}}\sum \mathbf{n_i z_i}^{\mathbf{2}} \qquad (2)$$

, where n_i is the number of ions with charge z_i. The summation is based on all the types of ions, i, in the formula unit. The SF_{GJ} values of BLnCs and BGLCs were calculated according to chemical composition and unit cell volumes listed in Table 3.

Table 3. Chemical composition, lattice parameters, structure factors of the Glasser–Jenkins equation (SF_{GJ}), and extended Goldschmidt tolerance factors (τ)[21] of BLnC and BGLC samples.

Sample	Composition	Space group	Lattice parameters				SF_{GJ} ($Å^{-1}$)	τ
			a (Å)	b (Å)	c (Å)	V ($Å^3$)		
BLC	$BaLaCo_2O_{5.63}$	Pmmm	3.898(5)	7.753(5)	7.727(5)	233.5(6)	21.57	4.054
BPC	$BaPrCo_2O_{5.64}$	Pmmm	3.871(5)	7.704(9)	7.526(9)	224.4(9)	21.96	4.066
BNC	$BaNdCo_2O_{5.57}$	Pmmm	3.893(1)	7.772(3)	7.609(1)	230.2(2)	21.11	4.069
BGC	$BaGdCo_2O_{5.55}$	Pmmm	3.872(1)	7.814(4)	7.529(2)	227.8(2)	21.00	4.084
BGLC37	$BaGd_{0.3}La_{0.7}Co_2O_{5.73}$	Pmmm	3.96(1)	7.75(1)	7.68(1)	236(2)	22.44	4.062
BGLC55	$BaGd_{0.5}La_{0.5}Co_2O_{5.79}$	Pmmm	3.899(1)	7.811(2)	7.614(2)	231.9(2)	22.92	4.068
BGLC82	$BaGd_{0.8}La_{0.2}Co_2O_{5.62}$	Pmmm	3.877(3)	7.792(7)	7.55(1)	227.9(7)	21.65	4.077

The modified tolerance factor introduced by Bartel et al. was also used to evaluate the structural stability of BLnC and BGLC perovskites. The extended Goldschmidt tolerance factor (τ) is defined as

$$\boldsymbol{\tau} = \frac{\boldsymbol{r_O}}{\boldsymbol{r_B}} - \boldsymbol{n_A}\left(\boldsymbol{n_A} - \frac{\boldsymbol{r_A}/\boldsymbol{r_B}}{\ln(\boldsymbol{r_A}/\boldsymbol{r_B})}\right) \qquad (3)$$

, where n_A is the oxidation state of A-site ions, r_A, r_B, and r_O represent the ionic radius of A-site and B-site cations and O anions ($r_A > r_B$ by definition). Perovskites are expected to have a τ value smaller than 4.18.[21] The τ values of BLnC and BGLC samples are listed in Table 3. To determine the average Co spin state at room temperature, XAS spectra at oxygen K-edge were measured as shown in Figure 2. As we reported previously, Co^{3+} exhibits a high spin (HS) state in BLC and an intermediate spin (IS) in BGC,[7] while the Co spin state of other compositions is intermediate. The edge for BGLC37 is located at a relatively low energy, suggesting that the majority of Co^{3+} in this composition is in an HS state. On the other hand, for BGLC55 and BGLC82, the edge appears at higher energies, indicating that more Co^{3+} exists in an IS state in these two BGLC samples with higher Gd content.

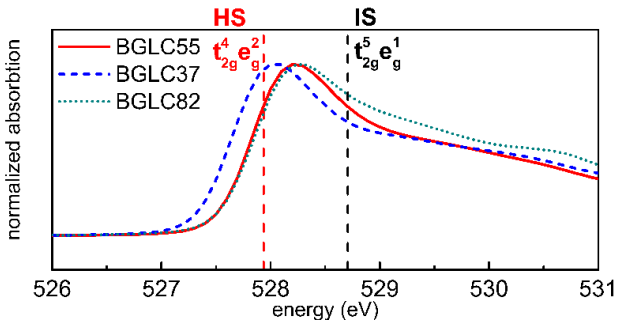

Figure 2. XAS spectra of oxygen K-edge of BGLC samples.

Thermodynamic Stability

The thermodynamic stability of double perovskite cobaltites (BLnCs and BGLCs) was determined by high temperature oxide

melt solution calorimetry. With the help of the thermodynamic cycles in Table 1, the enthalpies of formation from oxides ($\Delta H°_{f,ox}$) or elements ($\Delta H°_{f,el}$) were calculated from the enthalpies of drop solution (ΔH_{ds}). Lattice energies (U) were further calculated using Born–Haber cycles (Table S2 and S3). The results are listed in Table 4. As shown in Figure 3, $\Delta H°_{f,ox}$ values of all studied compositions are plotted as a function of the average ionic radius of trivalent lanthanide ions (Figure 3a),[22] structure factors of the Glasser–Jenkins equation[20] (Figure 3b), and extended Goldschmidt tolerance factors[21] (Figure 3c).

Table 4. Enthalpies of drop solution (ΔH_{ds}) in $3Na_2O{\cdot}4MoO_3$ at 800 °C, enthalpies of formation from oxides ($\Delta H°_{f,ox}$) or elements ($\Delta H°_{f,el}$) at 25 °C, and lattice energies (U) for BLnC and BGLC samples.

Sample	ΔH_{ds}[a] (kJ mol^{-1})	$\Delta H°_{f,ox}$ (kJ mol^{-1})	$\Delta H°_{f,el}$ (kJ mol^{-1})	U (kJ mol^{-1})
BLC	−7.29 ± 0.18 (8)	−221.98 ± 3.73	−2141.3 ± 4.5	−26471 ± 13
BPC	−13.21 ± 0.32 (5)	−193.95 ± 8.94	−2122.4 ± 9.3	−26655 ± 16
BNC	−11.11 ± 0.28 (8)	−186.49 ± 3.60	−2113.4 ± 4.5	−25921 ± 14
BGC	−25.07 ± 0.51 (8)	−161.54 ± 3.69	−2100.5 ± 5.0	−25808 ± 14
BGLC37	75.40 ± 0.61 (8)	−290.30 ± 3.70	−2215.5 ± 4.4	−27703 ± 13
BGLC55	−21.57 ± 0.37 (8)	−183.84 ± 3.64	−2113.0 ± 4.5	−28301 ± 13
BGLC82	35.77 ± 0.51 (8)	−230.23 ± 3.66	−2165.3 ± 4.7	−26583 ± 14

[a] Value is the mean of the number of experiments indicated in parentheses. Two standard deviations of the mean are given as errors.

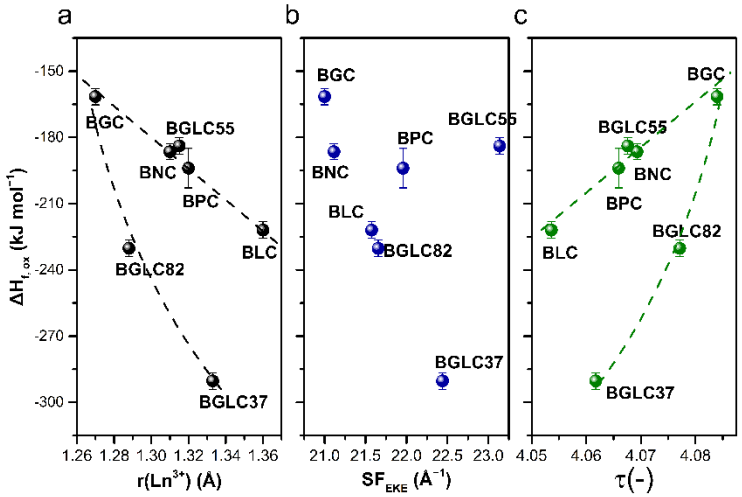

Figure 3. Enthalpies of formation from oxides ($\Delta H°_{f,ox}$) of BLnC and BGLC samples versus (a) the ionic radius of Ln^{3+} (CN=12), (b) the structure factor of the Glasser–Jenkins equation (SF_{GJ}), and (c) the extended Goldschmidt factor (τ)[21]. Curves are only to guide the eye and do not represent any physical fit of the data.

Table 5. Summary of enthalpies of drop solution in sodium molybdate (or lead borate for $La_{2-x}Sr_xCoO_{4-y}$ compounds) at 700 (ΔH_{ds}^{700}) or 800 °C (ΔH_{ds}^{800}), plus formation enthalpies of formation from oxides ($\Delta H°_{f,ox\text{-}CoO}$ and $\Delta H°_{f,ox\text{-}Co3O4}$ refer to formation enthalpies from CoO and Co_3O_4, respectively) at 25 °C for a range of cobalt-based perovskites

Stoichiometry	Av. ox. st. of Co	ΔH_{ds}^{700} (kJ/mol)	ΔH_{ds}^{800} (kJ/mol)	$\Delta H°_{f,ox\text{-}CoO}$ (kJ/mol)	$\Delta_{700/800}H°_{f,ox\text{-}Co3O4}$ (kJ/mol)
$La_{1.4}Sr_{0.6}CoO_4$	+2.6	83.63 ± 2.79[23]		−85.4[23]	−23.9
$La_{1.4}Sr_{0.6}CoO_{3.98}$	+2.56	80.20 ± 2.64[23]		−81.6[23]	−24.2
$La_{1.25}Sr_{0.75}CoO_4$	+2.75	94.16 ± 2.31[23]		−101.0[23]	−32.6
$La_{1.25}Sr_{0.75}CoO_{3.95}$	+2.65	74.21 ± 3.32[23]		−81.5[23]	−14.8
$LaSrCoO_{3.99}$	+2.98	102.35 ± 3.33[23]		−117.6[23]	−49.2
$LaSrCoO_{3.83}$	+2.66	67.92 ± 2.89[23]		−84.9[23]	−17.2
$La_{0.75}Sr_{1.25}CoO_{3.96}$	+3.17	101.93 ± 1.08[23]		−125.8[23]	−57.4
$La_{0.75}Sr_{1.25}CoO_{3.67}$	+2.59	42.76 ± 1.06[23]		−69.8[23]	−9.3
$La_{0.6}Sr_{1.4}CoO_{3.92}$	+3.24	104.33 ± 4.50[23]		−133.7[23]	−65.3
$La_{0.6}Sr_{1.4}CoO_{3.59}$	+2.58	39.30 ± 2.49[23]		−72.2[23]	−12.7
$La_{0.5}Sr_{1.5}CoO_{3.87}$	+3.24	99.31 ± 2.65[23]		−132.5[23]	−64.1
$La_{0.5}Sr_{1.5}CoO_{3.52}$	+2.54	25.36 ± 2.08[23]		−62.4[23]	−7.0
$LaCoO_3$	+3		28.73 ± 0.34[24]	−111.78 ± 1.36[24]	−43.40 ± 2.19

$LaCoO_{2.992}$	+2.98		28.72 ± 0.34[24]	−111.87 ± 1.36[24]	−43.49 ± 2.19
$La_{1.009}Co_{0.991}O_3$	+3		28.83 ± 0.34[24]	−113.40 ± 1.45[24]	−45.64 ± 2.27
$NdCoO_3$	+3		47.77 ± 1.05[24]	−98.33 ± 1.33[24]	−29.95 ± 2.16
$NdCoO_{2.985}$	+2.97		47.73 ± 1.05[24]	−98.49 ± 1.33[24]	−30.11 ± 2.16
$Nd_{1.009}Co_{0.991}O_3$	+3		47.73 ± 1.05[24]	−99.36 ± 1.34[24]	−31.60 ± 2.16
$SmCoO_3$	+3		53.25 ± 0.86[24]	−91.39 ± 1.46[24]	−23.01 ± 2.29
$SmCoO_{2.982}$	+2.96		53.19 ± 0.86[24]	−91.56 ± 1.46[24]	−23.18 ± 2.29
$Sm_{0.992}Co_{1.008}O_3$	+3		53.83 ± 0.91[24]	−90.34 ± 1.48[24]	−21.41 ± 2.31
$GdCoO_3$	+3		48.45 ± 0.95[24]	−87.83 ± 1.45[24]	−19.45 ± 2.28
$GdCoO_{2.968}$	+2.94		48.36 ± 0.95[24]	−88.16 ± 1.45[24]	−19.78 ± 2.28
$Gd_{1.006}Co_{0.994}O_3$	+3		48.55 ± 0.95[24]	−88.51 ± 1.46[24]	−20.54 ± 2.28
$YBaCo_4O_7$	+2.25	−90.83 ± 1.31[25]		−86.78 ± 3.65[25]	15.77 ± 4.19[25]
$YBaCo_3ZnO_7$	+2.33	−102.44 ± 1.08[25]		−72.78 ± 3.55[25]	29.77 ± 4.10[25]
$YBaCoZn_3O_7$	+3	−94.29 ± 0.40[25]		−76.13 ± 3.35[25]	26.42 ± 3.93[25]

On account of the large exothermic $\Delta H°_{f,\,ox}$ values, BLnC, and BGLC samples are thermodynamically stable relative to the corresponding binary oxides, among which BGLC37 and BGLC82 have great energetic stability. The trend of $\Delta H°_{f,\,ox}$ across the Ln series represents the result of the competition between lattice energies (U) of binary and complex oxides responding to the Ln contraction, which is generally associated with the coordination number of Ln^{3+}, i.e., the higher Ln coordination is accompanied by the smaller slope of U across the Ln series.[26] In the double perovskite structure, A-site Ln^{3+} ions are in 12-fold coordination, higher than the 7-fold or 6-fold coordinated Ln^{3+} ions in A-type (cubic) or C-type (hexagonal) Ln_2O_3. Therefore, there is an increase of Ln coordination in the formation of BLnCs from binary oxides, and the trend that $\Delta H°_{f,\,ox}$ becomes less exothermic as the Ln size decreases is generally found in such cases (Figure 3a). However, the more exothermic $\Delta H°_{f,\,ox}$ of BGLC37 and BGLC82 cannot be explained by the Ln size, and hence other factors should be taken into consideration. Since ionic interactions are influenced by the charge of ions (the term I in SF_{GJ}), a higher Co oxidation state along with fewer oxygen vacancies gives rise to stronger ionic interactions and more exothermic $\Delta H°_{f,\,ox}$. Indeed, oxidation must generally occur with a negative enthalpy change to compensate for the loss in entropy resulting from the incorporation of gaseous oxygen into a solid phase. In contrast, a larger lattice volume (the term V_m in SF_{GJ}) increases the cation-anion distance, resulting in weaker ionic interactions and less exothermic $\Delta H°_{f,\,ox}$. Figure 3b, shows the combined effect of the lattice volume, the Co oxidation state, and oxygen vacancies on the energetics of barium lanthanide cobaltites. The $\Delta H°_{f,\,ox}$ of BLC with δ = 0.1 obtained by Malyshkin et al. using room temperature solution calorimetry was −184.9 ± 14.7 kJ/mol [27], which is slightly less exothermic than the $\Delta H°_{f,\,ox}$ for BLC with δ = 0.37 (−221.98 ± 3.73 kJ/mol) in this study. As for BGC, the results obtained by Ivanov et al. show that as the oxygen nonstoichiometry (δ) increases, the $\Delta H°_{f,\,el}$ becomes less exothermic, e.g., −2027 ± 12 kJ/mol for δ = 0.488 and −1923 ± 5 kJ/mol for δ = 1.100,[28] while we got −2100.5 ± 5.0 kJ/mol for δ = 0.45. The same relation was reported by Tsvetkov et al.[29] for BNC and our result follows the trend that $\Delta H°_{f,\,el}$ becomes more exothermic with the lower δ value. In the case of BPC, the $\Delta H°_{f,\,el}$ value (−2122.4 ± 9.3 kJ/mol for δ = 0.36) obtained here is more exothermic than that reported by Ivanov et al. as −2072 ± 11 kJ/mol for δ = 0.32 [28]. This difference may come from the variable oxidation state of Pr. It was previously reported that 2–4 charge-type perovskites containing Pr are thermodynamically more stable than perovskites containing other tetravalent ions,[30] and this additional stability resulting from electronic factors may give a hint of different enthalpies of formation for BPC samples. From the structural point of view, the stability of perovskites can be evaluated by the means of the extended tolerance factor as reported by Bartel et al. [21]. In the studied materials, all samples exhibit tolerance factor values below 4.18, meaning that the perovskite structure is stable at room temperature, which is in line with their highly exothermic $\Delta H°_{f,\,ox}$. Regarding cobaltites containing Gd and La (BGLCs), decreasing stability occurs with higher Gd content, reflecting that the lower Co oxidation state is more favored for smaller Ln ions.[6] The deviation of BGLC55, however, may come from the properties of non-ideal solid solutions, (Figure 3b).

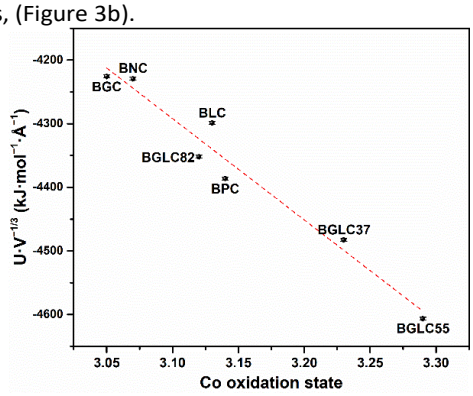

Figure 4. Lattice energy divided by cube roots of unit cell volumes ($U{\cdot}V^{-1/3}$) of BLnC and BGLC samples versus the Co oxidation state. By dividing lattice energies by cube roots of unit cell volume, we unify the values for the size effect of lanthanide ions. The red dashed line represents a linear fit (R^2 = 0.97) of all data, which is used to help compare the deviations from the trend and does not represent any physical meaning.

By comparing Tables 4 and 5, one can notice that the formation enthalpies of BGLC37 and BGLC82 are of strongly exothermic compositions, even if normalizing the Co content, indicating high stability of these compositions concerning other cobaltites. However, one should take into account varying oxidation states and electronic structure of Co, as well as oxygen non-stoichiometry, which may influence the formation energetics. An anomaly of mixing properties was reported by O'Neill and Navrotsky for Co_3O_4-containing spinel solid solutions[31] which was later found associated with a phase transition of Co_3O_4 at high temperature with a very large increase in entropy[32] The

transition is attributed to a partial change in electronic spin states of Co^{3+} from LS to a mixed spin state of LS and HS and is accompanied by a significant change in volume. $LaCoO_3$ exhibits a Co LS state and $La_{0.6}Sr_{0.4}CoO_4$ was reported to exhibit a Co HS state at elevated temperatures[33] while in the case of double perovskite cobaltites containing Ba and Ln, all studied samples exhibit a Co IS or HS state[7] To reveal the impact of Co spin states on the energetics, U values (calculated by Born–Haber cycles listed in Table S2) of BLnC and BGLC samples divided by the cube root of unit cell volumes ($U{\cdot}V^{-1/3}$) are plotted as a function of the Co oxidation state in Figure 4. Owing to the crucial role of the Co oxidation state in the energetics of barium lanthanide cobaltites, a roughly linear relationship is expected between $U{\cdot}V^{-1/3}$ and Co oxidation states in the narrow range, whereas some $U{\cdot}V^{-1/3}$ values locate off the fitted line. For example, BLC and BGLC37, having a Co HS state, shows a shift of U to the positive direction, while BGLC82 and BGC with an IS Co spin state have more exothermic $U{\cdot}V^{-1/3}$ values compared to the linear fitting. These deviations may hint that the Co spin state can contribute to the stability of Co compounds.

Stability in H_2O

The two separate sets of phenomena one stemming from thermodynamics and the second from the kinetics of material steam corrosion should be considered while forming conclusions. The degradation of air positrodes in PCECs is mainly caused by phase change, chemical mismatch, and cation interdiffusion[2]. Since we analyze here only stand-alone material the phase factor is of our interest. Therefore, we shall analyze both thermodynamics and kinetics inputs to general material stability in water vapor.

The stability of BLnCs and BGLCs was moreover evaluated under temperatures and pH_2O similar to operating conditions for PCE anodes. Chemical stability has been investigated for BGLC37 and BGLC82 at 400 °C and 1.5 bar H_2O, containing 0.24 bar of O_2 and balanced with Ar (1.26 bar), for 72 h. As shown in Figure 5, there is no change in PXRD patterns before and after the water vapor exposure for BGLC37 and BGLC82, confirming the stability in the given conditions. Rietveld refinement profiles show a good fit to the PXRD patterns using a single-phase double perovskite structure with orthorhombic symmetry (*Pmmm*). Unit cell parameters are summarized in Table S4. After increasing pH_2O to 10.5 bar at 300 °C for 100 h, secondary phases were found in BGLC37 and BGLC82 (Figure 6). For both samples, the main crystalline products of decomposition at high steam pressures are $Gd(OH)_3$ and $BaCO_3$ as well as Co compounds (Co_3O_4 and $Co(OH)_2$). Though, the existing $BaCO_3$ is the product of decomposition product BaO and/or $Ba(OH)_2$ reacting with either residual CO_2 in the gas mixture or CO_2 in atmospheric air before XRD measurements. Both compositions retain the main phase of the double perovskite structure. No reflections corresponding to the secondary phases containing La were identified in the PXRD patterns. However, a background increase was observed in the PXRD patterns after water vapor treatment, indicating the formation of amorphous hydroxides, which is more obvious after 10.5 bar of pH_2O for 100 h. This agrees with the recent Pan et al. study on $PrBa_{0.5}Sr_{0.5}Co_{1.5}Fe_{0.5}O_{5+\delta}$ (PBSCF)–$BaZr_{0.1}Ce_{0.7}Y_{0.1}Yb_{0.1}O_{3-\delta}$ (BZCYYb) composite positrodes in which they report that high steam concentrations promoted the segregation of Ba and Sr to the surface to form a Sr-OH or Ba-OH phase [34]. The simulation studies show that in the case of perovskites, the surface segregation can be enhanced also by the structural strain[35]. This can suggest that the compositional complexity of BLGC concerning BLnC can play a role in their stability in steam. Moreover, this can suggest that kinetics can play a crucial role in phase separation upon steam exposure.

Moreover, we tested BGLC37 composition at lower pH_2O but at a higher temperature (Fig. 7). This measurement shows that this composition is stable at these conditions. This shows the potential applicability of these compositions as positrodes operating in the range of temperatures 400 to 600 °C depending on the pH_2O.

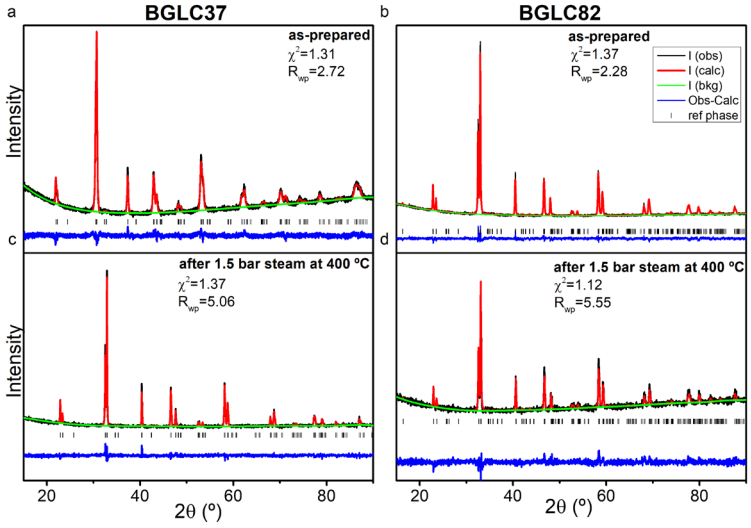

Figure 5. X-ray diffractograms with the Rietveld refinements of BGLC37 and BGLC82 before (a,c) and after (b,d) the water vapor treatment at 400 ºC and 1.5 bar of pH_2O for 72 hours (total pressure 3 bar, 1.26 bar Ar, 0.24 bar O_2).

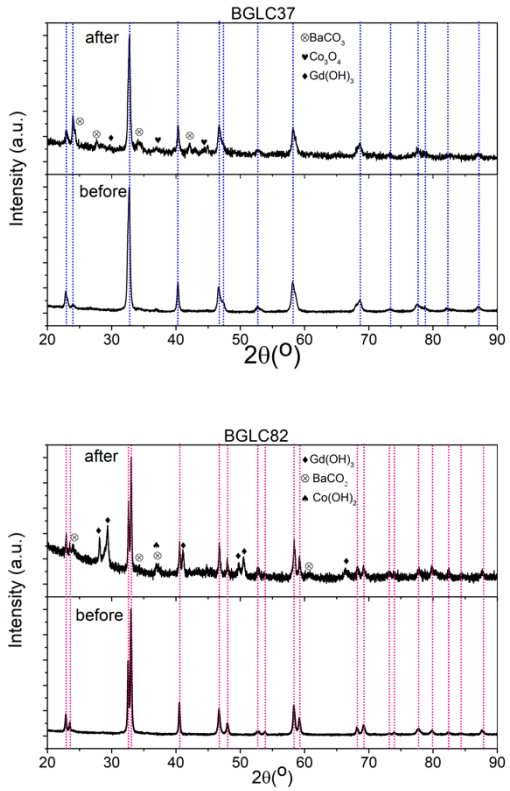

Figure 6. PXRD patterns of BGLC37 and BGLC82 before and after the water vapor treatment at 300 °C and 10.5 bar of pH_2O for at least 96 hours.

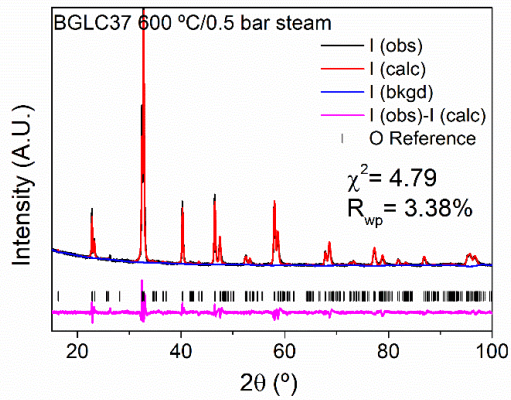

Figure 7. PXRD patterns of BGLC37 after the water vapor treatment at 600 °C and 0.5 bar of pH_2O for 72 hours.

SR-PXRD measurements were conducted to better characterize the phase content of BGLC82 after exposure to 10.5 bar of H_2O for 100 h at 300 °C. The data with the Rietveld refinement profile is depicted in Figure 8. According to the Rietveld refinement, in the post-exposure BGLC82 sample, the majority phase (44.6 mol%) is the double perovskite tetragonal structure (*P4/mmm*), along with $Gd(OH)_3$ (29.3 mol%), $BaCO_3$ (13.2 mol%), $Co(OH)_2$ (11.27 mol%), and $LaCoO_3$ (1.7 mol%) (this phase was below PXRD detection limit). The small amounts of precipitates containing La suggest that most La is retained within the perovskite structure. However, due to the low X-ray contrast between Ba, La, and Gd, it is not possible to reliably refine the cation composition of the double perovskite phase from the SR-PXRD data.

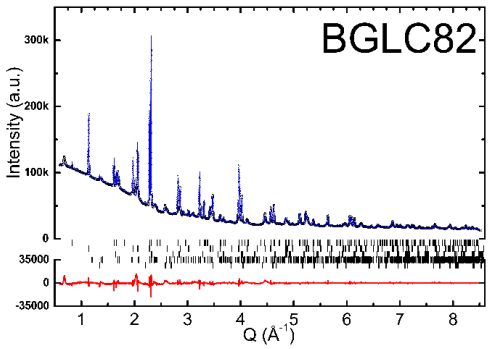

Figure 8. SR-PXRD pattern with the Rietveld refinement of BGLC82 sample exposed at 300°C and 10.5 bar of H_2O for 100 hours.

The stability of BLnC was studied by SR-PXRD. The results are depicted in Figure 9. All studied compositions were stable at high steam pressures, and no precipitates were visible in SR-PXRD patterns. There is a definite relation between the chemical composition and stability under high steam pressures. The difference between the samples with one large lanthanide – like La or Nd – and mixing in a smaller – like Gd – suggests that the relation of ionic radii of lanthanide can play the important role in stabilizing the perovskite structure towards H_2O.[32,33] The remaining double perovskite phase is possibly the more stable composition, meaning that the main perovskite phase persists even in higher steam pressures. We note that the observed "stability" in steam is governed by both thermodynamic and kinetic factors, the former defining what reactions are favorable, and the latter how fast they occur.

The thermodynamic study of the energetics of formation shows the higher stability of the materials with two lanthanides concerning the single lanthanide compositions, however, this trend is not followed for water steam experiments. On the other hand, the BGLCs series seems to fit the trend where BGLC73 is more stable than BGLC82 in both energetics of formation and water vapor experiments. However, one shall consider that this can be a case of different kinetics of materials corrosion for these two groups. Both BGLC73 and BGLC82 at higher vapor pressure partially decompose and additional phases are formed but the main perovskite phase persists. However, we are not able to determine the exact composition of the remaining double perovskite phase. It can be assumed, looking at the composition of precipitates (almost no La-containing phases), that the remaining is possibly BLC (or other BGLC phase with high La content) (Fig. 7 and 8). The persistence of only one of two end-members and be related to the higher thermodynamic stability of BLC in relation to BGC. The kinetics of decomposition of the BLC phase may be much slower than in the case of BGLCs.

This can be possibly caused by disorder/order present in phases containing two lanthanides. In such a case one should assume that the stability in a steam of a particular BLnC or BGLC phase is more governed by kinetics rather than thermodynamics. Especially in the view that all studied phases exhibit highly exothermic enthalpies of formation which makes them all quite thermodynamically stable. Moreover, the same is suggested by the values of the extended tolerance factor values.

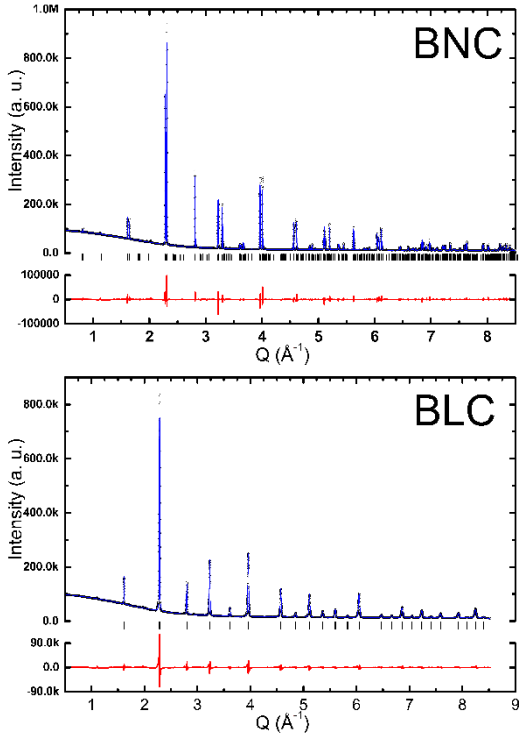

Figure 9. SR-PXRD patterns with Rietveld refinements of (a) BNC and (b) BLC samples exposed at 300°C and 10.5 bar of pH_2O for 100 hours.

Conclusions

The thermodynamic stability and high steam pressure stability of barium lanthanide cobaltites ($BaLnCo_2O_{6-\delta}$) and barium lanthanum gadolinium cobaltites ($BaGd_{1-x}La_xCo_2O_{6-\delta}$) have been evaluated in this work. All studied materials exhibit strongly exothermic enthalpies of formation from oxides, which implies their thermodynamic stability relative to binary oxides. The test under high steam pressure shows that BGLC37 and BGLC82 are performance stable (the main perovskite phase persists) up to 3 bars of water vapor at 400 °C and partially decompose to form some of the constituent oxides and hydroxides at 10.5 bar and 300 °C. However, BGLC37 is stable at 600 °C at 0.5 bars of steam. The higher negative formation energies for the BGLC compositions concerning the single-Ln compositions are not reflected in higher chemical stability under high steam pressures. Moreover, the cobaltites with one larger lanthanide (BNC and BLC) are stable up to 10.5 bars of steam partial pressure for as long as 100 hours.

Acknowledgments

The research has been supported by the National Science Centre Poland (2016/22/Z/ST5/00691), the Spanish Ministry of Science and Innovation (PCIN-2017-125, RTI2018-102161, and IJCI-2017-34110), and the Research Council of Norway (Grant n° 272797 "GoPHy MiCO") through the M-ERA.NET Joint Call 2016. We also acknowledge Solaris National Radiation Centre Poland for access to the XAS/PEEM beamline time (proposal no 201036). Dr. Chiu C. Tang at beamline I11 at Diamond Light Source, Didcot, UK is gratefully acknowledged SR-PXD measurements. The calorimetry at Arizona State University received financial support from the U.S. Department of Energy, Office of Basic Energy Sciences, Grant DE-SC0021987.

Authors' contribution

A.M-G – Writing – original draft; Conceptualization; Investigation; Supervision, Visualization, Methodology; Funding acquisition; Data curation; Project administration S. Y. – Writing – original draft; Investigation, Visualization; Data curation M.B. - Writing – original draft; Conceptualization; Investigation; Data curation R.S. – Writing – review & editing; Conceptualization, Supervision; Funding acquisition; Project administration M. H. S. – Writing – review & editing; Investigation; Funding acquisition; Resources; Project administration I. S. – Writing – original draft; Investigation, Visualization; Resources; Data curation A. W. - Writing – review & editing; Data curation; S. W. - Writing – review & editing; Investigation; J. M. S. – Supervision, Methodology; Project administration; Funding acquisition A. N. – Writing – original draft; Supervision; Methodology; Funding acquisition; Project administration M. G.- Writing – review & editing; Supervision

Notes and references

1 R. J. Braun, A. Dubois, K. Ferguson, C. Duan, C. Karakaya, R. J. Kee, H. Zhu, N. P. Sullivan, E. Tang, M. Pastula, A. Wood, T. Joia and R. O'Hayre, *ECS Trans.*, 2019, **91**, 997–1008.

2 C. Duan, J. Huang, N. Sullivan and R. O'Hayre, *Appl. Phys. Rev.*, 2020, **7**, 011314.

3 E. Vøllestad, R. Strandbakke, M. Tarach, D. Catalán-Martínez, M. L. Fontaine, D. Beeaff, D. R. Clark, J. M. Serra and T. Norby, *Nat. Mater.*, 2019, **18**, 752–759.

4 L. Q. Le, C. Meisel, C. H. Hernandez, J. Huang, Y. Kim, R. O'Hayre and N. P. Sullivan, *J. Power Sources*, 2022, **537**, 231356.

5 L. Q. Le, C. H. Hernandez, M. H. Rodriguez, L. Zhu, C. Duan, H. Ding, R. P. O'Hayre and N. P. Sullivan, *J. Power Sources*, 2021, **482**, 228868.

6 S. L. Wachowski, I. Szpunar, M. H. Sørby, A. Mielewczyk–Gryń, M. Balaguer, C. Ghica, M. C. Istrate, M. Gazda, A. E. Gunnæs, J. M. Serra, T. Norby and R. Strandbakke, *Acta Mater.*, 2020, **199**, 297–310.

7 I. Szpunar, R. Strandbakke, M. H. Sørby, S. L. Wachowski, M. Balaguer, M. Tarach, J. M. Serra, A. Witkowska, E. Dzik, T. Norby, M. Gazda and A. Mielewczyk-Gryń, *Materials*, 2020, **13**, 4044.

8 I. Szpunar, S. Wachowski, T. Miruszewski, K. Dzierzgowski, K. Górnicka, T. Klimczuk, M. H. Sørby, M. Balaguer, J. M. Serra, R. Strandbakke, M. Gazda and A. Mielewczyk-Gryń, *J. Am. Ceram. Soc.,*, 2020, **103**, 1809–1818.

9 E. Vøllestad, M. Schrade, J. Segalini, R. Strandbakke and T. Norby, *J. Mater. Chem. A*, 2017, **5**, 15743–15751.

10 R. Strandbakke, V. A. Cherepanov, A. Yu. Zuev, D. S. Tsvetkov, C. Argirusis, G. Sourkouni, S. Prünte and T. Norby, *Solid State Ion.*, 2015, **278**, 120–132.

11 K. Conder, E. Pomjakushina, A. Soldatov and E. Mitberg, *Mater. Res. Bull.*, 2005, **40**, 257–263.

12 A. Navrotsky, *J. Am. Ceram. Soc.*, 2014, **97**, 3349–3359.

13 M. W. Chase, *J. Phys. Chem. Ref. Data, Monograph*, 1998, **9**, 1–1951.

14 W. Gong and A. Navrotsky, *J. Mater. Res.*, 2019, **34**, 3337–3342.

15 A. Mielewczyk-Gryn, S. Wachowski, K. I. Lilova, X. Guo, M. Gazda and A. Navrotsky, *Ceram. Int.*, 2015, **41**, 2128–2133.

16 R. J. M. Konings, O. Beneš, A. Kovács, D. Manara, D. Sedmidubský, L. Gorokhov, V. S. Iorish, V. Yungman, E. Shenyavskaya and E. Osina, *J. Phys. Chem. Ref. Data*, 2014, **43**, 13101.

17 A. Mielewczyk-Gryn and A. Navrotsky, *Am. Mineral.*, 2015, **100**, 1578–1583.

18 Y. Zhang, I.-H. Jung, *Calphad*, 2017, **58**, 169–203.

19 S. P. Thompson, J. E. Parker, J. Potter, T. P. Hill, A. Birt, T. M. Cobb, F. Yuan and C. C. Tang, *Rev. Sci. Instrum.*, 2009, **80**, 075107.

20 L. Glasser and H. D. B. Jenkins, *J. Am. Chem. Soc.*, 2000, **122**, 632–638.

21 C. J. Bartel, C. Sutton, B. R. Goldsmith, R. Ouyang, C. B. Musgrave, L. M. Ghiringhelli and M. Scheffler, *Sci. Adv.*, 2019, **5**, 1–10.

22 R. D. Shannon, *Acta Crystallogr. A*, 1976, **32**, 751–767.

23 T. R. S. Prasanna and A. Navrotsky, *J. Mater. Res.*, 1994, **9**, 3121–3124.

24 S. K. Sahu, S. Tanasescu, B. Scherrer, C. Marinescu and A. Navrotsky, *J. Mater. Chem. A*, 2015, **3**, 19490–19496.

25 D. S. Tsvetkov, P. S. Maram, N. S. Tsvetkova, A. Y. Zuev and A. Navrotsky, *J. Phys. Chem. A*, 2018, **122**, 9597–9604.

26 S. Yang, A. Anderko, R. E. Riman and A. Navrotsky, *Acta Mater.*, 2021, **220**, 117289.

27 D. A. Malyshkin, V. V. Sereda, A. L. Sednev-Lugovets, I. L. Ivanov, D. S. Tsvetkov and A. Yu. Zuev, *J. Electrochem. Soc.*, 2022, **169**, 024511.

28 I. L. Ivanov, D. A. Malyshkin, N. S. Tsvetkova, V. V. Sereda, E. A. Kiselev, A. Y. Zuev and D. S. Tsvetkov, *Thermochim. Acta*, 2014, **578**, 28–32.

29 D. S. Tsvetkov, R. E. Yagovitin, V. V. Sereda, D. A. Malyshkin, I. L. Ivanov, A. Y. Zuev and A. Maignan, *Solid State Ion.*, 2021, **361**, 115549.

30 A. Navrotsky, W. Lee, A. Mielewczyk-Gryn, S. V. Ushakov, A. Anderko, H. Wu and R. E. Riman, *J. Chem. Thermodyn.*, 2015, **88**, 126–141.

31 H. S. C. O'Neill and A. Navrotsky, *Am. Mineral.*, 1984, **69**, 733–753.

32 H. S. C. O'Neill, *Phys. Chem. Miner.*, 1985, **12**, 149–154.

33 Y. Orikasa, T. Ina, T. Nakao, A. Mineshige, K. Amezawa, M. Oishi, H. Arai, Z. Ogumi and Y. Uchimoto, *J. Phys. Chem. C*, 2011, **115**, 16433–16438.

34 J. Pan, Y. Ye, M. Zhou, X. Sun and Y. Chen, *Energy Fuels*, 2022, **36**, 12253–12260.

35 J. W. Han, H. Jalili, Y. Kuru, Z. Cai and B. Yildiz, *ECS Trans.*, 2011, **35**, 2097–2104.